Meteorologische Zeitschrift, Vol. **24**, No. 1, 83–97 (published online January 13, 2015)

The role of orography in the regeneration of convection: A case study from the convective and orographically-induced precipitation study

Victoria H. Smith[1,2*], Stephen D. Mobbs[1,2], Ralph R. Burton[1,2], Matt Hobby[1,2], Fumiko Aoshima[3], Volker Wulfmeyer[3] and Paolo Di Girolamo[4]

[1]Institute for Climate and Atmospheric Science, University of Leeds, Leeds LS2 9JT, UK
[2]National Centre for Atmospheric Science, UK
[3]Institute of Physics and Meteorology, University of Hohenheim, Germany
[4]Dipartimento di Ingegneria e Fisica dell 'Ambiente, Universitá degli Studi della Basilicata, Italy

(Manuscript received July 25, 2012; in revised form June 12, 2014; accepted June 25, 2014)

Abstract

A case study that took place during the Convective and Orographically-induced Precipitation Study (COPS) is presented. A squall-line embedded with convective precipitation, which was associated with the outflow boundary of a mesoscale convective system (MCS) regenerated above the crests of the Black Forest. This followed an initial decay of convection as the MCS descended in the lee of the Vosges to cross the Rhine valley. High resolution simulations using the WRF numerical model will demonstrate that the Black Forest mountains were instrumental in causing significant modification to the distribution and intensity of convection in the region. Fine scale detail of the orography was, however, found to be unimportant. Instead, modelling errors are attributed to poor boundary layer representation.

Keywords: COPS, Convection regeneration, Orography, WRF

1 Introduction

Various mechanisms have been identified for the enhancement and modification of convection by orography, and for the influence of orography on the timing and location of convective precipitation. Banta (1990) classified these mechanisms into 3 groups:

1. Forced uplift, resulting from the flow encountering the orographic barrier, causing the air to be lifted to the level of free convection (LFC).
2. Generation of thermal flows due to differential heating of the orographic surfaces.
3. Aero Dynamic effects such as blocking and deflection.

The relative importance of the above mechanisms depends on many factors. Crook and Tucker (2005) noted that a crucial effect of each mechanism is to induce convergence and lifting of boundary-layer air either directly through orographic lifting, or via thermally-generated baroclinicity. It is common that for any particular orographic region, different forcing mechanisms will be important according to factors such as the synoptic situation, wind direction and speed, static stability, and time of day. Morcrette et al. (2007) describe how a shower, which later developed into an isolated thunderstorm in the southern United Kingdom, initiated when the interaction of a synoptic-scale and a surface-forced mesoscale convergence line combined, making the development of the thunderstorm highly predictable. Analysis of the case was furthered by Lean et al. (2009), who found that descent of post-frontal flow in the lee of Dartmoor caused a hole to develop in the layer cloud aloft. Enhanced radiation then produced sufficient additional surface heat and moisture flux for a thunderstorm to develop downstream of the orography. The authors noted that consolidation of the various available forcing mechanisms was required for the thunderstorm to initiate.

The Black Forest is known to frequently induce thermally-driven flow systems during the summer. This enables plain-mountain flows to generate east of the Black Forest, causing convergence lines to form both above the mountains and in their lee when the synoptic flow is westerly (Kalthoff et al., 2009). The region is therefore favourable for convection initiation and intensification (Barthlott et al., 2006; Meissner et al., 2007), and the region south of Stuttgart was found to be the most frequent (and intense) location for severe hailstorms in a study by Kunz and Puskeiler (2010). The forecasting of such events remains challenging for numerical weather prediction models and several field campaigns have taken place to gain better understanding of the processes involved in order to improve forecasting skill. Notable campaigns include the International H_2O

*Corresponding author: Victoria Smith, Institute for Climate and Atmospheric Science, University of Leeds Leeds, UK, e-mail: victoria.smith@ncas.ac.uk

Project (IH0P_2002) (Weckwerth et al., 2004), which took place in the mainly flat or gently rolling Southern Plains of America in 2002. Also in 2002, the Vertical Exchange and Topography (VERTIKATOR) (Barthlott et al., 2006) project aimed to quantify the influence of orography and land use on the initiation of shallow and medium convection in the region of the Black Forest. In summer 2004, the Convective Storm Initiation Project (CSIP) (Browning et al., 2007) investigated initiation processes associated with the complicated coastline and undulating hills of south west England in summer 2005.

The Black Forest, along with the more westerly Vosges mountains was chosen to be the inner study domain of the Convective and Orographically-induced Precipitation Study (COPS) (Wulfmeyer et al., 2008) during summer 2007, to *"advance the quality of forecasts of orographically induced convective precipitation by four-dimensional observations and modelling of its life cycle"*. The two mountain ranges are separated by the Rhine valley, and the orography is complicated further by intersecting valleys with widths of tens to hundreds of metres.

One objective of COPS was to investigate the impact of orography on deep moist convection (DMC). The study presented here endeavours to address this aim using multi-platform observations and high resolution modelling, through investigation of convection regeneration (CR) above mountain crests, and the subsequent intensification of convective cells in the lee of the mountains. Three simulations have been undertaken using the Weather Research and Forecasting (WRF) numerical model to elucidate the role of the COPS orography on convection regeneration during Intensive Operation Period (IOP) 9c, which occurred on 20 July 2007. One simulation used a realistic representation of the Black Forest, to asses WRFs ability to reproduce the observations of the case and to investigate the processes that led to CR above the mountain crests. The lee-side intensification of convective cells was an important aspect of IOP 9c because the subsequent organisation of the cells into a mature squall line of thunderstorms caused flooding in eastern Germany later that day. We also use WRF to investigate the role convergence of thermally-driven flows with the MCS played in assisting this downstream development. Two idealised simulations were conducted to investigate the relative importance of orography in triggering CR. The first replaced the majority of the Black Forest with a plain of altitude equal to that of the Rhine valley to investigate *if* the mountains were responsible for CR in the model. The second replaced the inner domain orography with a two-dimensional ridge to remove the complexity of the real mountains and assess whether valley flows played a critical regenerative role, or simply served to influence downstream development and intensification of convection.

The outline of the paper is as follows. Section 2 presents observations of the case. Section 3 describes the WRF model setup. Section 4 presents our results, where we first asses the ability of WRF to reproduce convection initiation above the mountain crests. The role of orography in CR is then discussed in section 4.2 and 4.3 by comparing the control simulation with the two idealised model runs. The key findings from this paper are summarised in section 5 and conclusions drawn in section 6.

2 Case overview

Comprehensive analyses of both the synoptic situation and meso-scale observations for IOP 9c are presented in Corsmeier et al., (2011), hereafter C11. Only a brief description of the case and further observations that assist the model verification of *this* study only are presented here.

During the morning of 20 July 2007, a north-easterly propagating and well organised MCS crossed the orographically complex COPS study region. During this time, the structure and intensity of convection embedded within the outflow region of the MCS was altered through interaction with the orography, which can be seen from the time series of German weather service (DWD) rainfall radar composites in Fig. 1. As the southern end of the MCS reached the COPS domain (region within red rectangle), the radar composite at 0927 UTC (1a) shows how the southern part of the squall-line was less intense than further north. The section of the MCS that encountered the COPS orography was therefore already decaying. Descent in the lee of the Vosges further accentuated this and by 1026 UTC (1b) no precipitation was falling onto the Rhine Valley. At this time however, individual cells of precipitation are clearly visible above the crests of the northern Black Forest. Further downstream 1c shows that by 1241 UTC these cells have merged to form an intense line as the southern part of the squall line crossed central southern Germany.

30 Automatic Weather Stations (AWS) were operational in the northern Black Forest on 20 July 2007 and observations of near surface potential temperature and 1 minute averaged (from 1 Hz data) horizontal winds in Figure 2 show the passage of the MCS. At 0936 UTC, (2a), strong winds (with a maximum of approximately $20\,\mathrm{ms}^{-1}$) on the upper western slopes of the mountains corroborate the arrival of a gust front ahead of the main system. By contrast, low wind speeds in the Rhine valley and low-lying western Black Forest indicate that the outflow was elevated. This occurred because a very stable layer of fog had developed in the Rhine valley overnight, preventing the MCS outflow from reaching the valley floor. By 0948 UTC, (2b), the gust front had propagated to the centre of the Black Forest. Strong down-valley winds observed by AWSs in the north-south aligned Murg valley indicate that the valley channelled the flow. As the gust front reached and passed the mouth of the valley however, the flow was forced up the Murg valley and into the heart of the northern Black Forest. By 1000 UTC (2c), the radar echoes show that convection had regenerated directly above the mountain crests. By

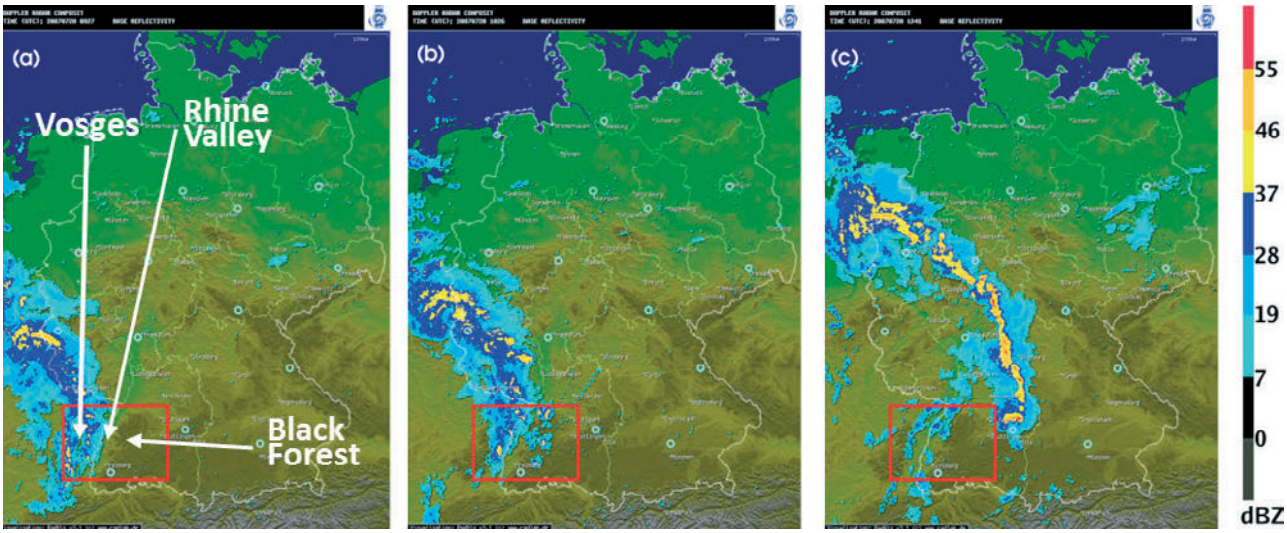

Figure 1: DWD rainfall radar composite indicating precipitation over Germany at (a) 0927, (b) 1026, and (c) 1241.

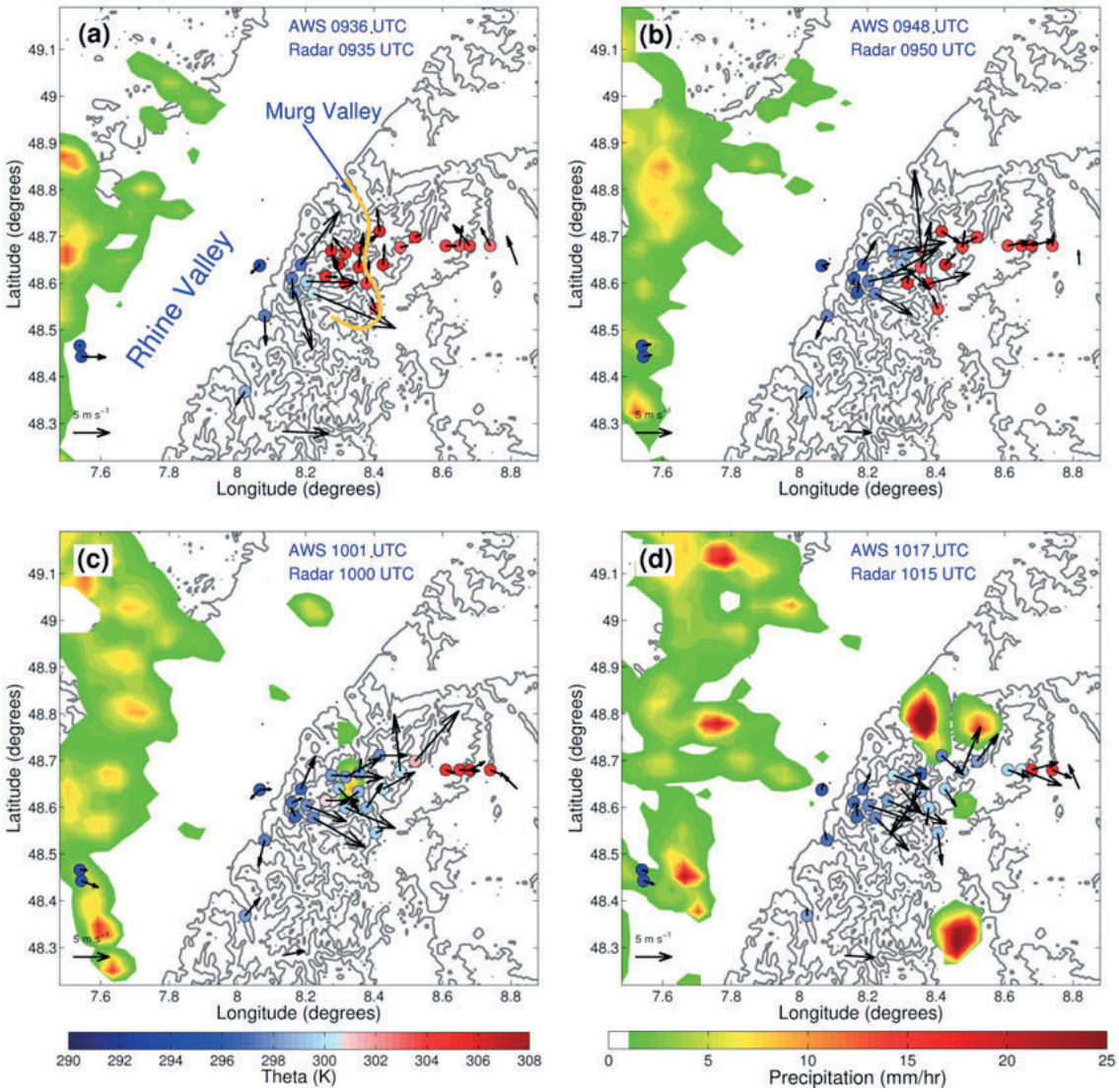

Figure 2: Surface potential temperature (K, filled circles) and horizontal wind vectors (ms^{-1}) observed by AWSs in the Rhine valley and northern Black Forest, and precipitation (mm/hr, filled contours) observed by the German composite (DX) radar. Grey contours show topography every 200 m. The orange curve on 3a denotes the approximate path of the Murg Valley.

Table 1: Numerical and physical configuration of WRF. For a more detailed description of the physical schemes used, see Skamarock et al., 2008.

	Domain 1	Domain 2	Domain 3
Horizontal resolution	2.7 km	900 m	300 m
Timestep (s)	12	6	2
Cumulus parameterisation	Betts-Miller-Janjic	None	None
Microphysics	Morrison (double moment)		
Diffusion / turbulence	2nd order horizontal diffusion with 1st order Smagorinsky closure for K		
LW Radiation	Rapid Radiative Transfer Model (RRTM)		
SW Radiation	Dudhia – allows for cloud and clear sky absorption and scattering		
Surface Layer	Standard Monin-Obukhov similarity functions		
Land surface	Soil temperature only (5 layers)		
Boundary-layer	Yonsei University – explicit entrainment and parabolic *k* profile in mixed layer		

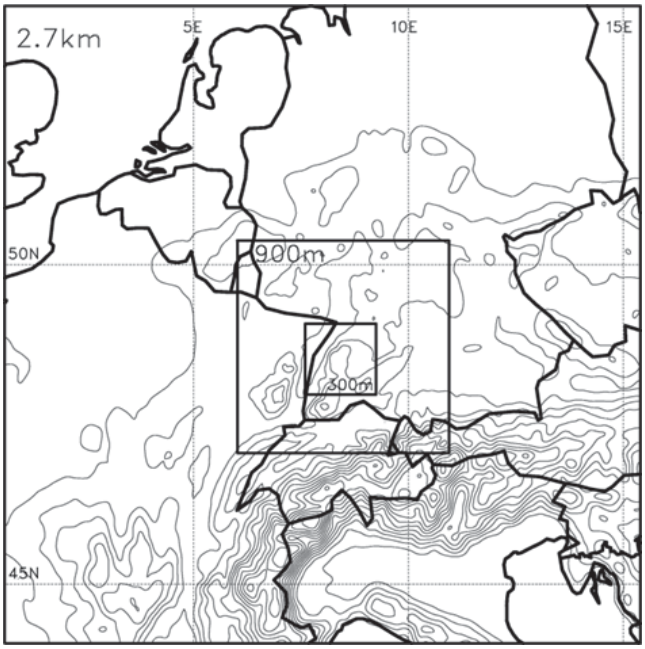

Figure 3: Model domains used in this study. Contours show topography with intervals every 250 m.

1017 UTC (2d), flow in the Murg valley had reversed entirely. The valleys of the northern Black Forest were now channelling the flow into the lee. Throughout the morning, clear skies enabled strong radiative heating of a region between the Black Forest and the Swabian Jura that can be characterised as an elevated plain. This in turn led to the generation of a plain-mountain flow towards the Black Forest and convergence east of the mountains. The effect was to intensify the regenerated convective cells, which then went on to form the squall-line observed in 1c.

3 Methodology

3.1 Model description

The WRF numerical model is a fully compressible, non-hydrostatic mesoscale model with terrain-following co-ordinates (Skamarock et al., 2008). This study used version 3.0.1.1 and was run with three nested domains, each comprising 400 × 400 grid points. The inner domain was centred over the northern Black Forest. Initial and lateral boundary conditions were provided by 0.25 ° ECMWF analyses at 0000 UTC on 20 July 2007, and were interpolated onto a grid with 120 vertical levels. Nudging of the lateral boundary conditions on the outer domain was applied at each time step through linear interpolation of the six hourly analyses data. A summary of parameterisations used and model setups is given in Table 1.

3.2 Control run

WRF has been used in this study for two purposes. A control simulation first assesses the ability of WRF to reproduce observed convection regeneration. The three domains for this simulation are shown in Figure 3, and the middle and inner domains in 4a. It was not possible to include the Vosges mountains in the inner domain due to computational limitations, but this was not viewed to be problematic because the resolution of the middle domain, which *did* included the French mountains, remained sufficiently high to be convection permitting. The model run was begun at 0000 UTC on 20 July to allow sufficient 'spin up' before the time of interest and was run for 18 hours. The performance of this simulation has been evaluated by comparing wind fields, cloud (formation) and precipitation locations, profiles and convective activity between the model and the available observations. The control simulation will henceforth be referred to as R1. Results are presented in section 4.1.

3.3 Modified orography

Two further idealised simulations use WRF to investigate the specific role of the Black Forest in CR.

R2: To investigate *if* the Black Forest was essential for convection regeneration on 20 July 2007, all but the outer 50 grid points of the inner domain orography were replaced by flat terrain roughly equal in height to that of the Rhine Valley. This removed approximately 75 % of the Black Forest (4b). The outer 50 grid points provided a transition zone for interpolating the idealised topography back towards the real topography at the domain edge. The width of the Rhine valley was effectively increased from approximately 35 km to approximately 100 km, and the eastern edge of the enlarged valley was now terminated by the orography of the Swabian Jura. Because WRF uses a terrain-following co-ordinate system and generates its initial conditions by interpolating the comparatively course 0.25 ° (~ 18.5 km) and 91 vertical level ECMWF analyses, the idealistic atmosphere

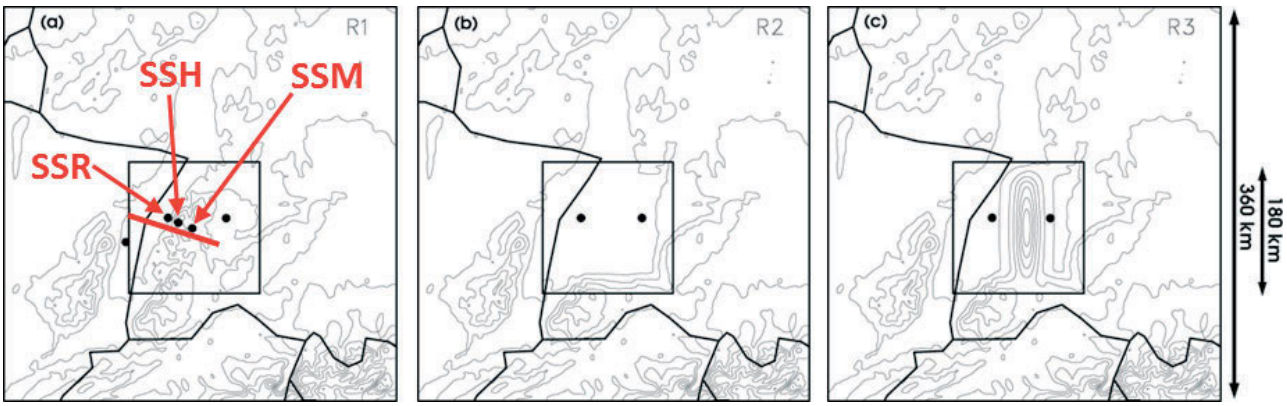

Figure 4: Contours of topography every 200 m for the middle and inner model domains of each of the model runs. (a) is the control run with real orography in the inner domain (R1), (b) is the idealised no orography in the inner domain (R2) and (c) is the idealised run with an idealised ridge (R3). Black dots show the locations of all COPS supersites in R1 and the equivalent locations of supersites R and S in R2 and R3. The red line in 5a shows the location of cross sections in Figure 10.

was created through the standard vertical interpolation and extrapolation method as detailed in section 5.2.3 of Skamarock et al., (2008), which interpolates using functions of dry pressure step-wise from the model lid towards the surface.

R3: Observations showed that valleys within the Black Forest were important for channelling flows. By replacing the real orography with an idealised ridge we investigate whether the role of valleys was solely to influence the downstream development and intensification of convection, or to also assist with convection regeneration above the mountain crests. In R3 the orography of the inner domain was replaced by a three-dimensional ridge (4c) with the geometry

$$h_{\mathrm{sfc}} = \frac{h}{(1 + (x/a)^2 + (y/b)^2)} \qquad (3.1)$$

where h_{sfc} is the terrain height, h the maximum height of the orography (1000 m) and x and y are the distances (in km), east and north of the lower-left hand corner of the inner domain, respectively. a and b are the half width (5 km) and half length (50 km) of the ridge. These dimensions were chosen to create a ridge that best matched the geometry of the Black Forest. The outer 50 grid points were again used as a transition zone between the real and idealised topography.

The R1 land surface properties were inspected for the region whose orography was modified in R2 and R3, and the most common was used as the uniform land use type for the modified orography areas. The resultant land use for the modified orography regions was duly set to be deciduous forest.

4 Results

4.1 Control WRF simulation

We must first point out that R1 reproduced features of the MCS propagation later than they were observed. This is attributed to errors in the synoptic scale initial conditions because after initiation, WRF was only forced from the boundaries and synoptic development subsequently evolved without additional data assimilation. Comparison of WRF with the observations has therefore been conducted when key features (for example, the gust front reaching the western flank of the Black Forest, convergence in the lee, and precipitation) occur in the same locations and *not* at the same times. Overlays of cloud, precipitation and surface wind in Figure 5 show the leading edge of the MCS cloud bank and the high winds of the outflow in approximately the same location before the gust front reaches the Western slopes of the Black Forest. WRF simulates two lines of convection that don't extend as far south as the observations. In both the observations and R1, a south-easterly plain-mountain thermal flow is developing, although the lee slope flow in WRF is more southerly. Additionally, the simulated wind field upstream of the Black Forest is stronger than that generated from Vienna Enhanced Resolution Analysis (VERA, Steinacker et al., 2006).

The profiles in Figure 5 show good agreement between R1 and the observations throughout the majority the troposphere, indicating that WRF mostly simulated the vertical structure well. The dry bias in R1 above 600 hPa is attributed to errors introduced by the input data. The boundary-layer profiles clearly differ however. Low level saturated air (indicating fog in the Rhine Valley) and a strong temperature inversion in the observed profile are absent R1. Conversely, WRF failed to reproduce any fog. A poorly represented boundary-layer in WRF might be explained by the use of the Yonsei University (YSU) boundary-layer scheme (Hong et al., 2006) which allows turbulent fluxes to depend on local mean gradients. It works by diagnosing an expected boundary-layer depth then instantaneously mixing values throughout the entire layer (Weisman et al., 2008). The YSU scheme uses a first order, non-local countergradient term coupled with an entrainment term, the latter being proportional to the surface buoyancy flux. The

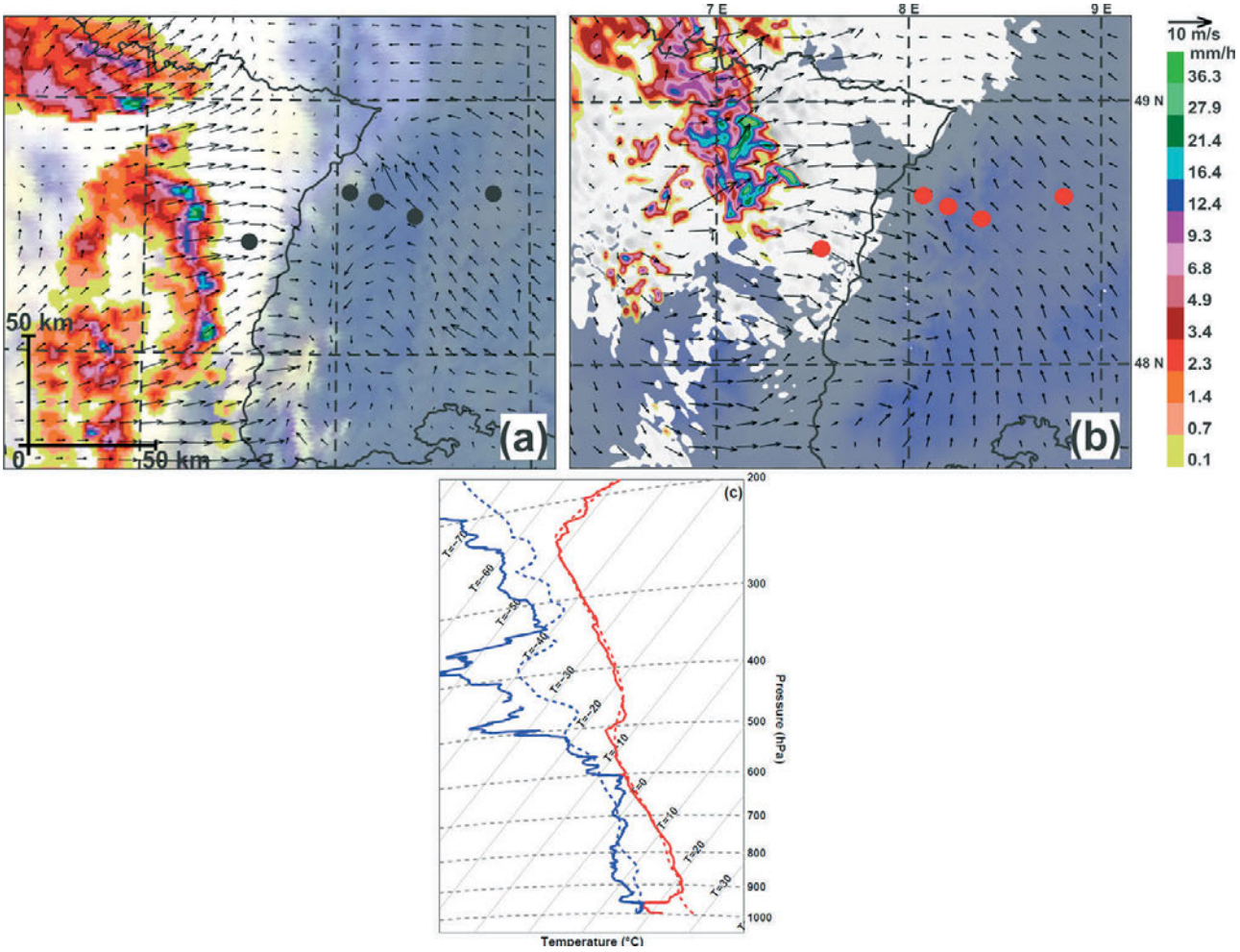

Figure 5: (a) Observed cloud cover from Meteosat Second Generation (MSG) images and DWD DX radar data (product of DWD radar composite and radar quality product composite) (filled contours mm/h); and Vienna Enhanced Resolution Analysis (VERA) surface wind vectors at 0900 UTC. (b) Equivalent fields from domain 2 of R1 at 1000 UTC. Column integrated cloud hydrometeors (white / grey shading), precipitation (filled contours mm/h) and surface horizontal wind vectors. Topography is depicted in (a) and (b) by the background blue/grey colour. The dots indicate COPS supersites. (c) Shows vertical profiles of temperature (red) and dew point temperature (blue) from SSR. The solid lines are observations made by a radiosonde launched at 0908 UTC. The dashed lines are R1 data at 1000 UTC.

top of the BL is determined by a critical Richardson number of zero and the YSU scheme is constructed so that turbulent fluxes of heat and moisture are not identically zero in regions of zero mean gradient. For a full description of the YSU scheme and its implementation in WRF, see Hong et al. (2006), WRF Technical note. Its efficacy has been investigated in Weisman et al., (2008) and Burton et al., (2013). The first study found that the YSU scheme created drier and deeper boundary-layers, and was particularly "aggressive" in eroding temperature inversions. The latter found that the YSU scheme significantly overestimated boundary-layer depth. We suspect that this aggressive mixing prevented the formation of the observed inversion and fog. Higher order TKE and more sophisticated boundary-layer schemes were unavailable when the simulations were undertaken so unfortunately it wasn't possible to test this hypothesis. One hour later (Figure 6), the observed radar retrievals (6a) show that convection had regenerated above the crests of the northern Black Forest (circled). Three regions of simulated precipitation above the crests of the mountains in R1 at 1100 UTC (6b) indicate that despite errors in the boundary-layer representation, WRF simulated the regenerated convection. In the southern-most of the circled cells, the maximum upward and downward wind speeds simulated were 3.0 ms^{-1}, and $-1.1\,ms^{-1}$, respectively, at an altitude of approximately 5 km, which are comparable to the in-situ aircraft observations described in Corsmeier et. al (2011).

Figure 7 compares the observations and R1 at 1100 and 1200 UTC, respectively, to see whether or not WRF reproduced the observed lee-side convection intensification. Readers should note that 7c shows profiles from the more easterly Super-site Murg (SSM) (see Figure 3a). The line of cloud in the lee of the orography was mostly reproduced (7b). However, the cloud doesn't extend as far south and less precipitation was generated. We believe that there are two reasons for this.

(I) Stronger westerly flow dominated the southern part of the R1 domain, forcing the lee-side thermally-

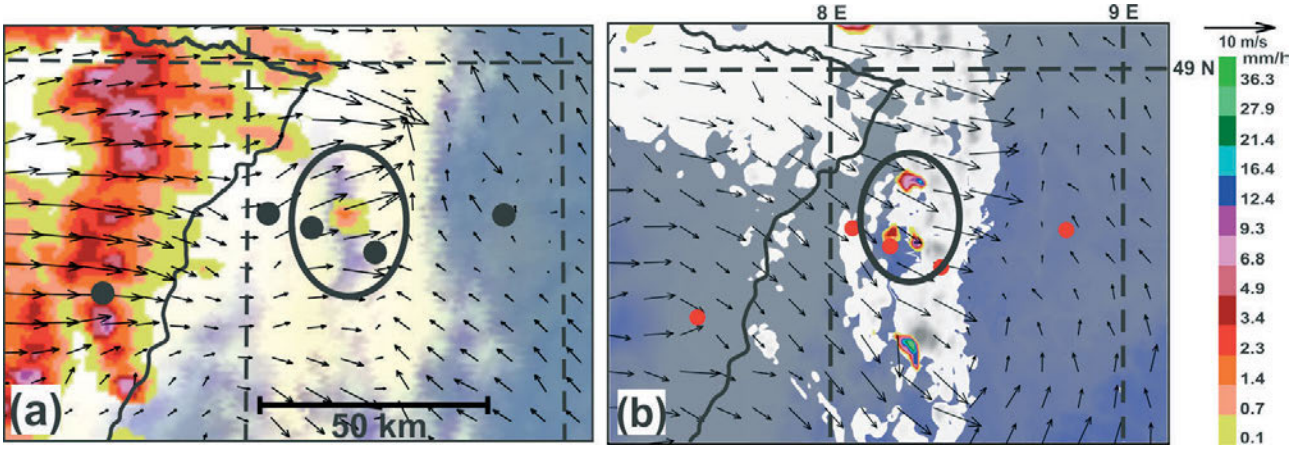

Figure 6: Same as Fig. 5a and b but at 1000 UTC (a) and 1100 UTC (b), and for a smaller region.

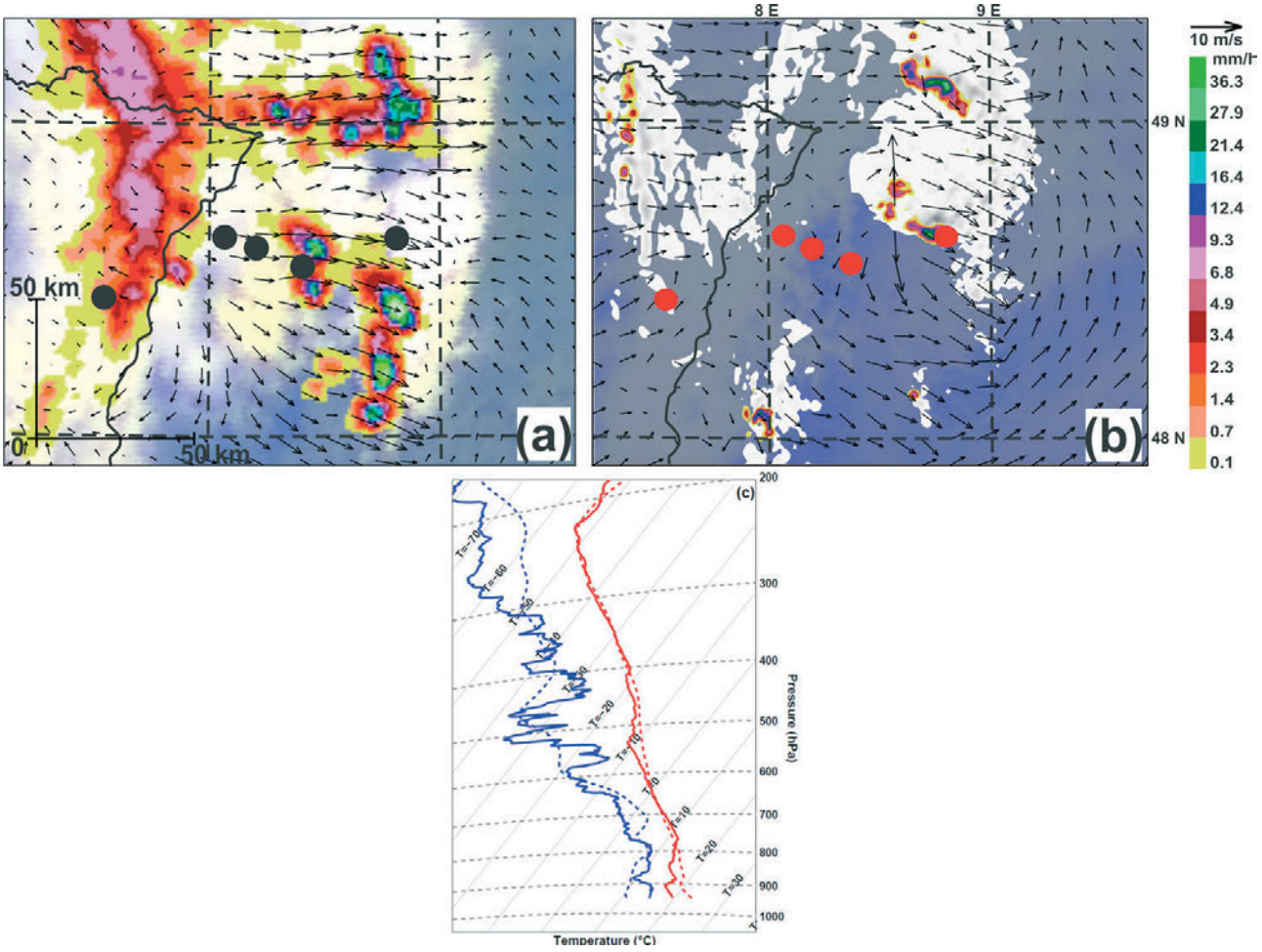

Figure 7: (a) and (b) are the same as Fig. 5a and b, but at 1100 UTC at 1200 UTC, respectively. (c) is the same as Fig. 5c but from SSM. The observed profile is from a radiosonde launched at 1127 UTC and the R1 profile is from 1200 UTC.

driven flow to be deflected. The simulated winds east of the Black Forest were consequently more southerly than observed. Surface convergence in WRF was therefore weaker, reducing the contribution of convergence in strengthening convection that had regenerated above the mountain crests.

(II) The profiles in 7c show that the boundary-layer (at SSM) has deepened with a height of approximately 780 hPa, but WRF is again drier than the observations, reducing the potential for clouds to form. The difference is less pronounced than the earlier profile at SSR but this is because a fog layer had not been present at SSM and

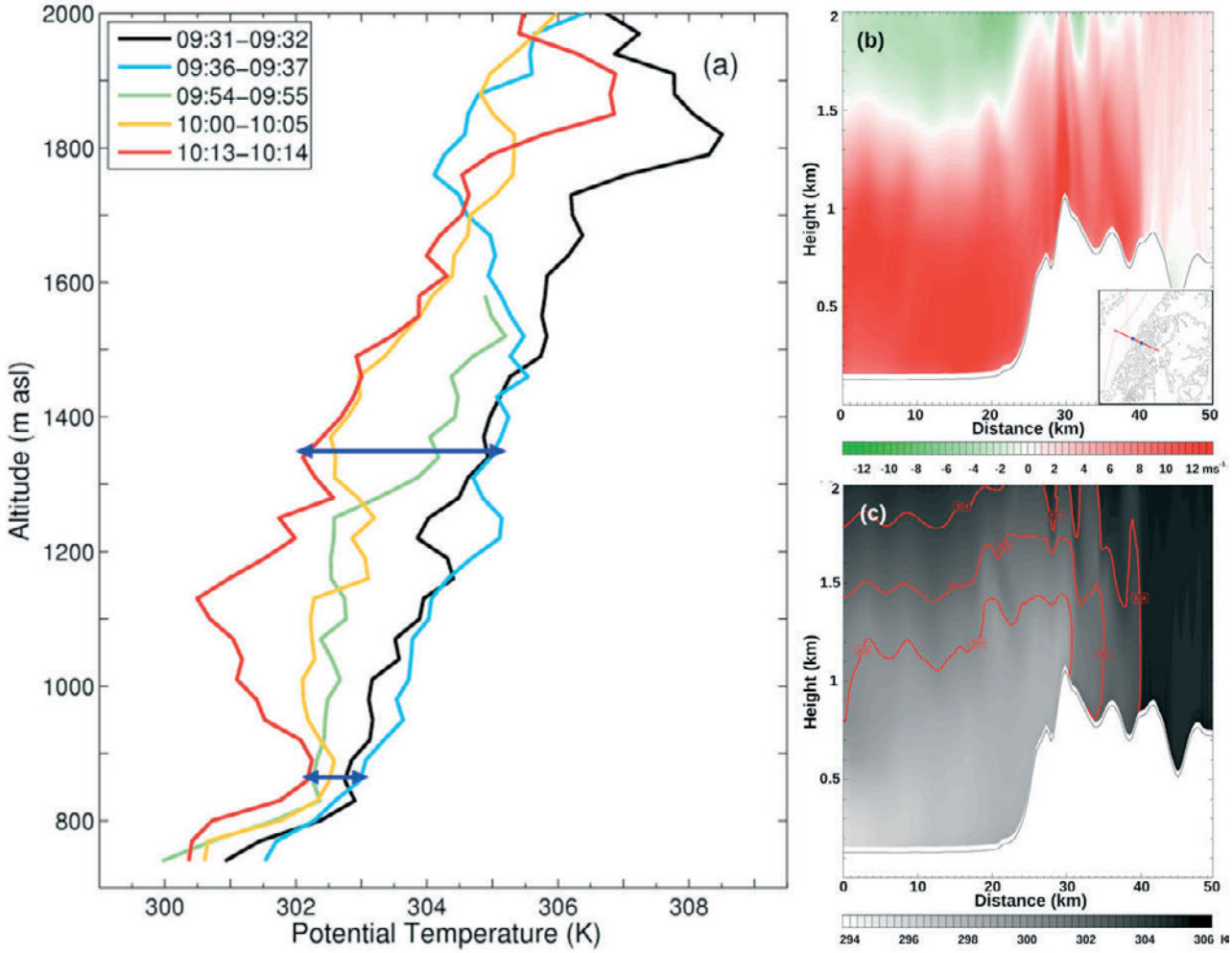

Figure 8: (a) Observed temperature profiles between 800 m and 2 km, from the University of BASILicata Raman Lidar system (BASIL; DI GIROLAMO et al., 2009) at SSR between 0931 and 1041 UTC, and (b) 50 km long cross sections of horizontal wind speed and (c) potential temperature through the Rhine Valley and Black Forest mountains from R1 at 1040 UTC. In (b), red (green) colours indicate westerly (easterly) flow, and the red lines in (c) indicate the 300 (lowest curve), 302 and 304 K isotherms. The inserted figure in b shows the location of the cross section within D03, with SSR and SSH identified by the blue bullets.

because the boundary layer development had evolved throughout the morning.

The skill of WRF to reproduce the case has been further investigated through comparison of R1 with profiles of observed θ from SSR between 0931 and 1041 UTC (Figure 8). Immediately following the gust front arrival (8a, black and blue curves), θ in the boundary layer increased gradually with height. It is not until 1000 UTC (yellow curve) that the observations show evidence of colder air arriving above ~ 850 m. The observations show that over a period of 45 minutes, little cooling (1 K) had taken place just below mountain height (850 m, lower blue arrow). Over the same period, a 3 K cooling had taken place at 1300 m (upper blue arrow). The delay between the gust front and the arrival of elevated cold air implies that the cold outflow air was blocked by the mountains and forced to build up against the western slope of the Black Forest. A wind speed cross section through super sites R, H, M and S at 1040 UTC (8b) shows that the gust front, with wind speeds in the region of 10–12 ms^{-1} and indicated by the grey curve, had travelled 10 km across the mountains at this time. Although the corresponding θ plot shows some cold air immediately behind the gust front (behind the 304 K isotherm in 8c), the 300 K isotherm (lower red line) shows that the main body of the cold outflow air still remained upstream of the Black Forest and had been lifted almost 300 m above the mountain top. R1 therefore supports the blocking concept, and separation of the gust front and the cold air of the outflow. It should be noted that the observed θ profile in 8a between 1013 and 1014 UTC, shows rapidly decreasing θ between approximately 900 m and 1200 m asl (red line). This feature was observed during one profile only, suggesting that it is transient. Later profiles are unavailable due to low cloud cover and precipitation.

The differences between the observations and R1 must be considered when interpreting the effect of the orography on convection. Convection *did* regenerate above the crests of the Black Forest however, and we

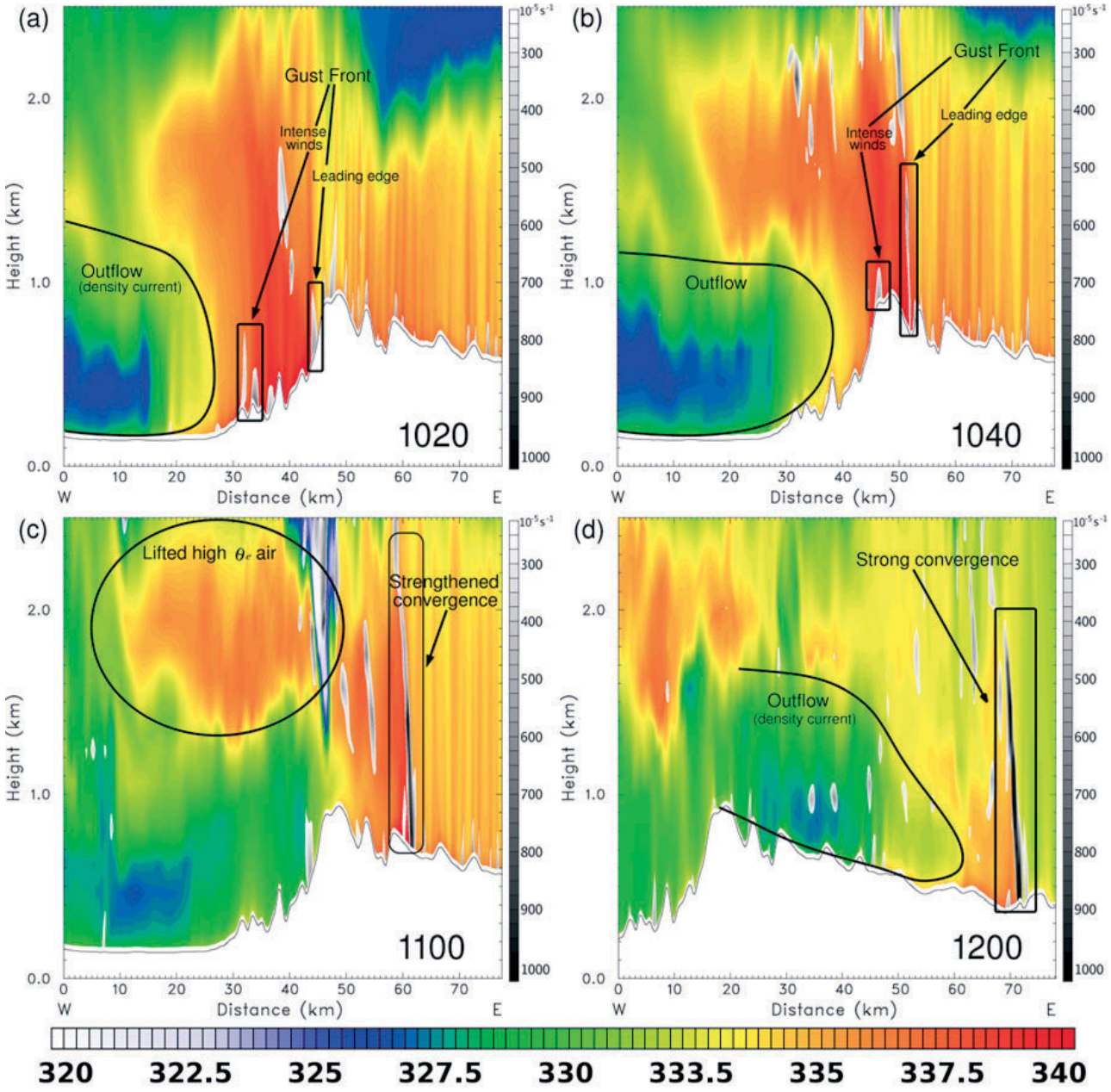

Figure 9: Cross sections of equivalent potential temperature (background colour shading) and convergence (grey shading) from R1. Slices are across the Rhine Valley and northern Black Forest (see Figure 4), at 1020 (a), 1040 (b), 1100 (c) and 1200 UTC (d). 10d is slightly further East.

therefore conclude that despite the errors, WRF exhibits the necessary skill for investigating initiation mechanisms. The presence of clouds and a reduced precipitation similarly located to reality, together with a highly comparable flow structure for the majority of the domain and similar temperature and moisture profiles confirm that WRF has reproduced the key features of the propagation of the MCS and CR.

4.2 Role of orography in convection regeneration

From Figure 9a, two regions of convergence upstream of the mountain crests identify the leading edge of the gust front and the strongest winds (from un-shown data) ahead of the outflow in R1. The gust front precedes a tongue of low θ_e air, which is the outflow flowing across the valley as a density current. Twenty minutes later, (9b), the outflow has undercut high θ_e air, lifting it above the height of the Black Forest. By 1100 UTC, (9c), the gust front has been forced over the mountains. Surface convergence has now strengthened. This is because upon reaching the lee of the orography, the westerly outflow converged with a southerly / south-easterly flow. The observed and simulated lee slope flows deviate significantly. Contrary to the observations, WRF fails to generate a thermally-driven upslope flow. In section 4 we described how the boundary layer parameter-

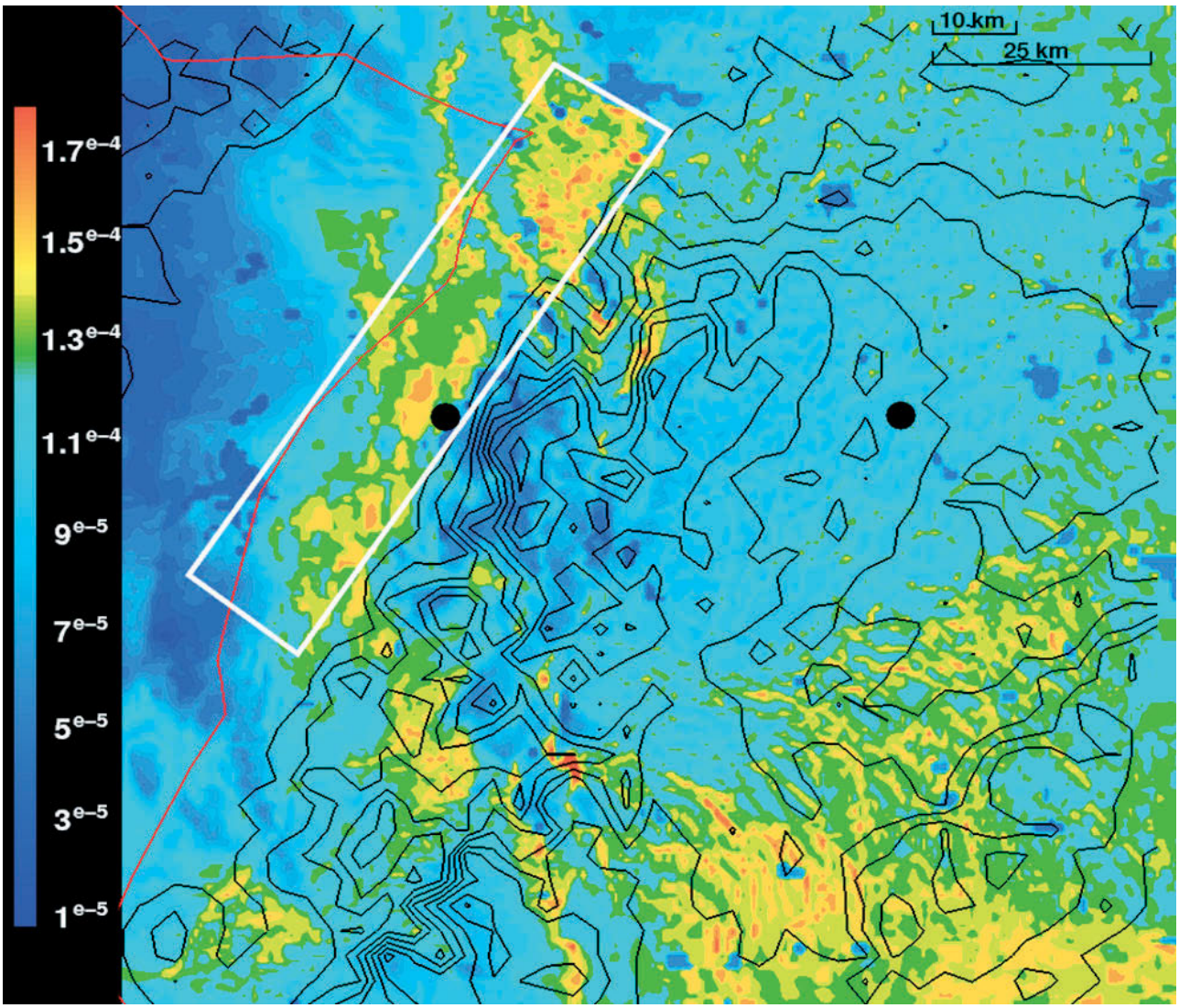

Figure 10: Surface moisture flux ($kgm^{-2}s^{-1}$) and topography (m) for the inner domain of R1 at 1040 UTC. Topography contours are shown every 200 m. The black dots show the location of supersites R and S.

isation used vertically mixed variables throughout the entire layer. This would effectively reduce the temperature gradient between the mountains and the plain east of the Black Forest and consequently reduce the strength of any thermally-driven flow. Despite the model error, the convergence line *did* strengthen (9c and 9d).

Behind the gust front, 9c shows that lifted high θ_e air is an isolated feature above the western slope of the Black Forest between approximately 1.5 km and 2.3 km. Comparison of 9c with an identical cross section of θ (not shown), revealed that this was due to higher moisture. Convergence alone cannot increase θ_e therefore its origin has been investigated by looking at the surface moisture flux (Figure 10). A region of higher moisture flux can be seen west of the Black Forest (within white box), where approximately $1.5^{e-4}\,kgm^{-2}s^{-1}$ of water was being transported into the boundary layer. Over a two hour period, this would equate to the transfer of just over $1\,kgm^2$. We suggest that the θ_e anomaly resulted from the undercutting and lifting of this moisture-enriched air. The isolated high θ_e air in 9b and 9c contains cells of strong vertical velocity (not shown), indicating that the forced uplift and increased moisture were sufficient for convection to initiate. By 1200 UTC, 9d shows that elevated high θ_e air above the mountain crests has largely been removed

4.3 Modified orography

The results of R2 will be discussed first to establish if uplift of warm and moist valley air from the undercutting outflow would have provided enough uplift for CR, or if extra forcing from orographic uplift was required. The impact of removing the complex nature of the Black Forest (R3) will then be analysed in section 4.3.2.

4.3.1 R2 – flat terrain

The inner domain surface θ_e and horizontal winds of R1 at 1100, 1120 and 1140 UTC (Figures 11a–c) show the

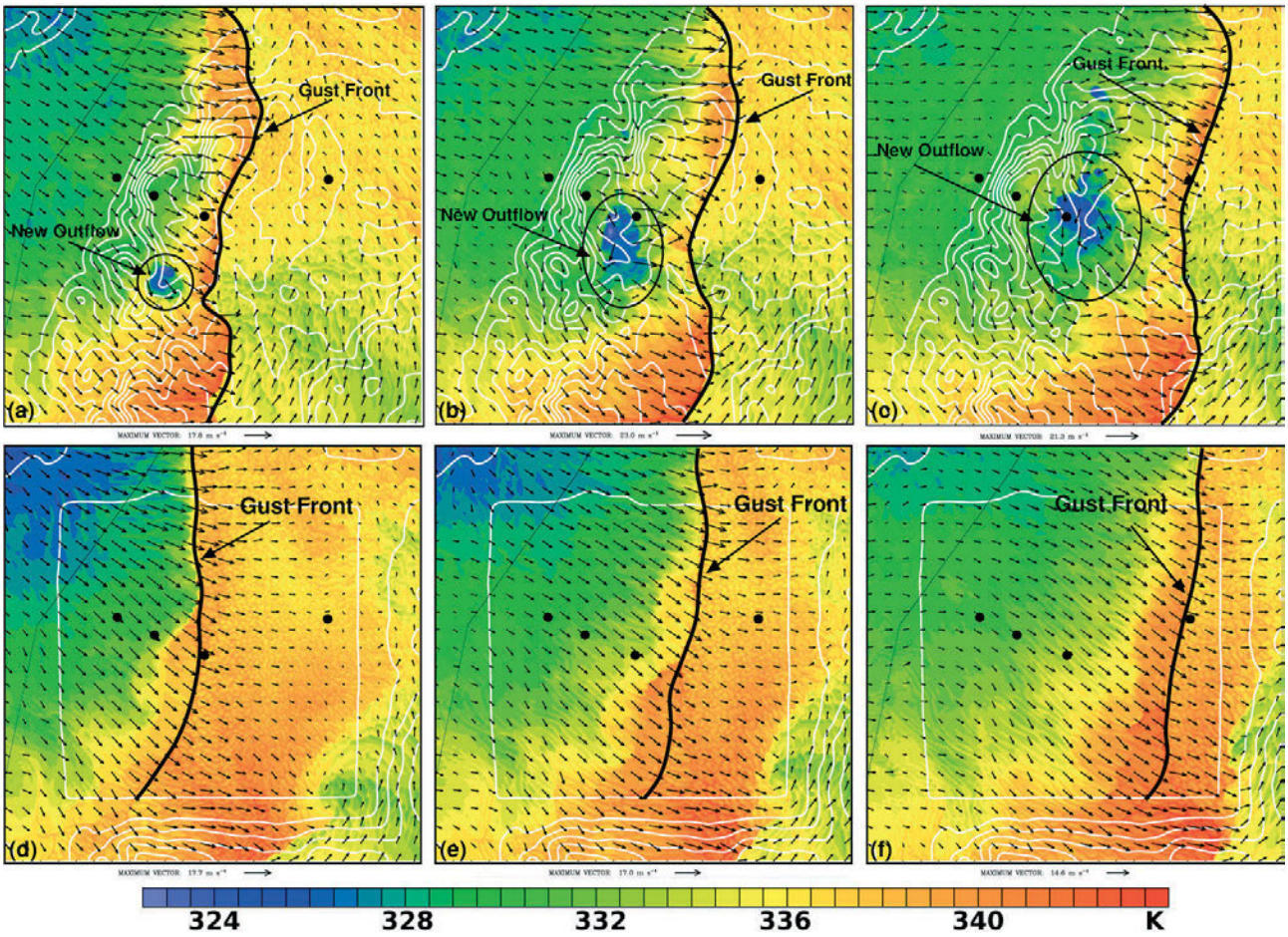

Figure 11: Surface Θ_e (background colour), horizontal wind vectors and topography (white contours) for the inner domain (120 × 120 km) of R1 (a–c) and R2 (d–f) at 1100 (left column), 1120 (middle column) and 1140 UTC (right hand column). The black dots show the location of super-sites R, H, M and S in the upper panel and super-sites R and S in the lower panel.

downdraft from a regenerated convective cell intensifying as it propagates across the domain. By contrast, the corresponding results from R2 (Figures 11d–f) show that when the inner domain orography was removed, convection failed to regenerate. The strongest surface winds are also weaker and structurally less well organised in R2 than R1. A gust front has been identified from the location of the strongest winds in R2; however, it is less well defined than that of R1. In R1, the gust front also appears to be well coupled with the cold air of the MCS outflow but in R2, (particularly in the southern part of the domain); the strongest winds are approximately 40–50 km further east of the outflow. Winds in this more southerly part of the R2 domain are also stronger than further north, and occur where the outflow encounters the Alps implying that the presence of orography was fundamental for strengthening and modifying the gust front. Comparison of R1 at 1100 UTC, (11a), with observations of the gust front at 10 UTC (lower left panel of Figure 9 in C11), and the fact that no distortion and strengthening was simulated in R2 confirms that the Black Forest orography was essential for the evolution of the gust front. Propagation of the MCS outflow across the now larger valley floor can be seen in Figure 12. In common with Figure 9 (R1), warm moist air was undercut and lifted by the outflow. The distance over which the outflow travelled before reaching the orography in R1 was only 35 km, and uplift was further enhanced upon reaching the Black Forest when the outflow was forced over the mountains. Convection then regenerated above the mountain crests. In R2 the valley is approximately 100 km wide and the outflow was able to cross the domain as an undisturbed density current. Without additional forced uplift from orography, lifting of the warm moist air by the density current was insufficient for convection to regenerate. By 1200 UTC (12d) the outflow has propagated across the domain and evolved into a density current approximately 800 m deep.

In Figure 12d the MCS gust front had propagated across the flat domain and now reached the orography of the Swabian Jura in central southern Germany. Convergence above the western slopes of the orography indicates that upon reaching orography, a stronger gust front was generated. An overlay of surface winds, convergence and precipitation at 1240 UTC in Figure 13 shows that the convergence line has now become distorted; much in the same way that the shape of the observed and R1 gust front was modified when it reached

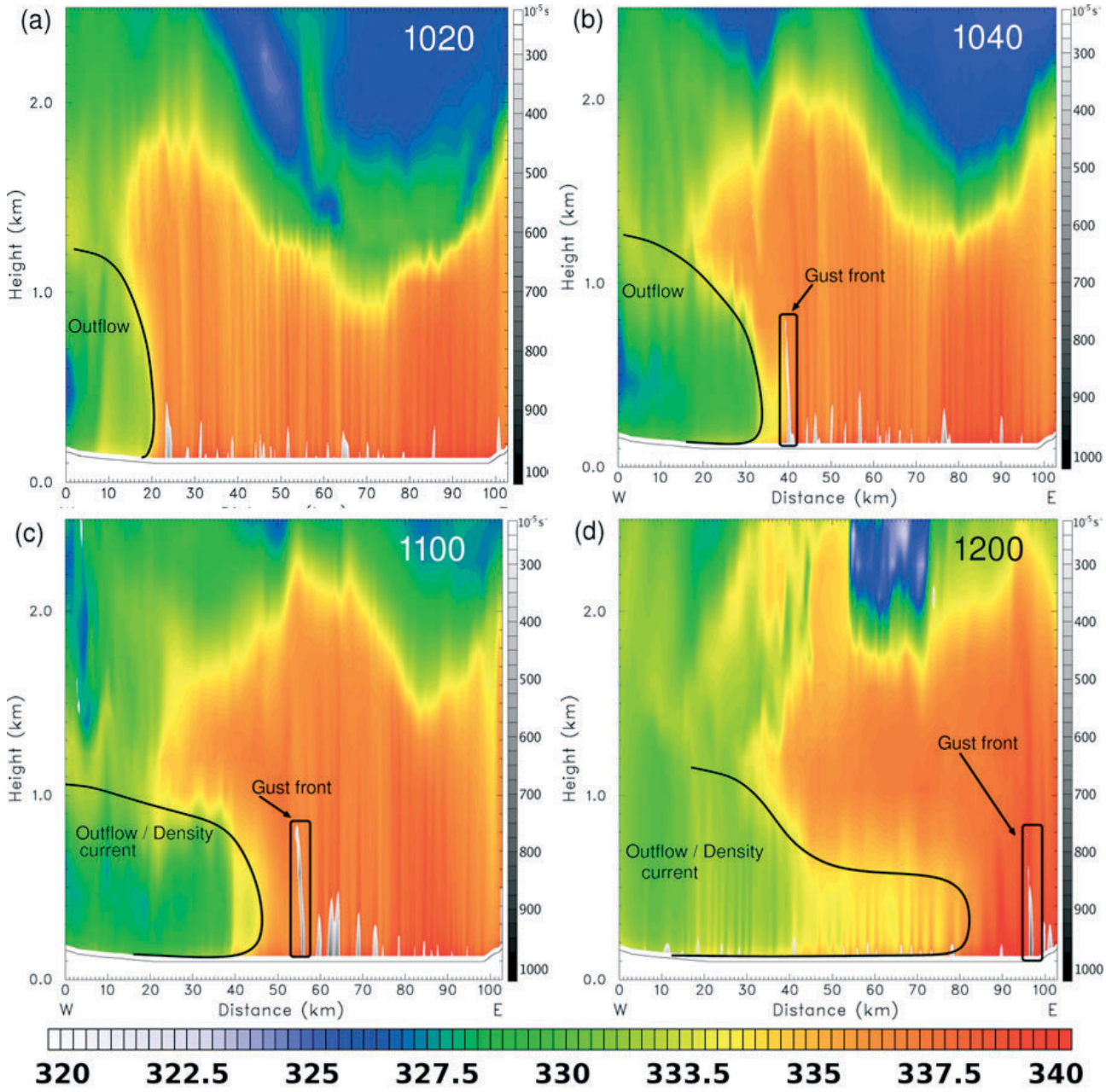

Figure 12: Same as Figure 9, but for R2 and a slightly larger (102 km) cross section.

the western slopes of the Black Forest (lower left panel of Figure 9 from C11 and Figure 11a, respectively). The convergence line in Figure 13 again follows the shape of the orography, which enforces the notion that the orography caused the intensification and organisation of the outflow. Two regions of convection can be seen in Figure 13, the northern-most of which has precipitated. As soon as the propagating MCS outflow encountered some orography, the combination of strengthening convergence and elevated warm moist air led to CR.

4.3.2 R3 – idealised ridge

Analysis of R3 will be undertaken by comparing an overlay of surface winds, convergence and precipitation from a section of the intermediate domain at 1120 UTC, (Figure 14a) with an equivalent plot from R1, (14b). An important difference between the inner domains of the two simulations is that the R3 orography is steeper and more uniform. Steeper orography and a more uniform barrier should enhance the convergence line intensification, resulting in stronger convection. The time of 1120 UTC was chosen for comparison because CR was strongest at this time in R1. Three features are immediately apparent from Figure 14:

1. CR in R3 produced more intense precipitation.
2. Convection extended further south.
3. R3 more closely reproduces the observed flow features than R1.

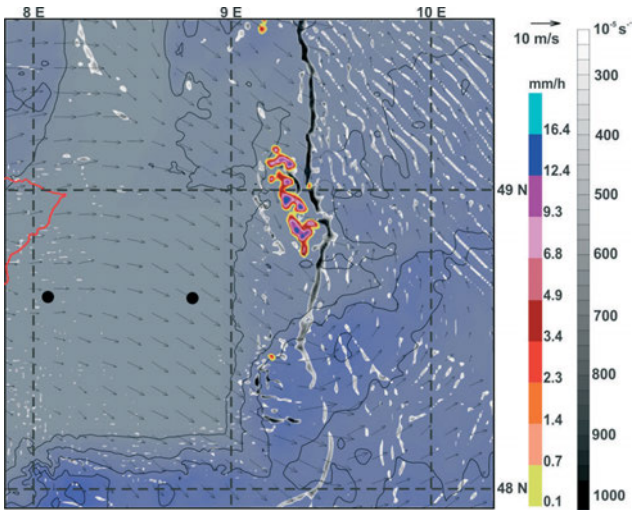

Figure 13: Wind vectors (ms^{-1}), convergence (s^{-1}) and precipitation (mm/h) at 1240 UTC from a section of domain 2 of R2. Background colour and black contours (200 m intervals) are topography, and black dots are supersites R and S.

More intense convection was anticipated because of extra lifting from the steeper and consistent orography. It wasn't expected, however, for the convergence line and subsequent convection to extend further south (14a) than in R1 (14b). The more southerly convergence line in R3 can be explained with closer interpretation of the surface winds. The southern part of the ideal orography dropped in altitude and the high ground did not therefore merge with the remaining real orography of the southern Black Forest as in reality. The effect was to create a new valley, allowing the outflow to flow *around* the southern end of the idealised orography (red arrow in 14a). In R1 (14b), the air was forced to flow over the orography. The direction of the channelled flow in R3 was perpendicular to the south-western Swabian Jura. Convergence resulted, forcing the overall convergence line to extend further south. The extended convergence line in the model was thus generated by a different mechanism to that observed. The flow and convective features are more consistent with the observations in R3 than R1 and R2, but for different reasons.

5 Summary of forcing mechanisms

The modelling in this study has established that convection initiated when elevated warm and moist air, convergence and strong updrafts were combined, but triggering could only occur in response to orographic lifting.

Simulation of the case showed that as the MCS outflow propagated across the Rhine valley, it undercut warm, moist valley air, and lifted it above the height of the orography. Ahead of the outflow, a pronounced gust front and narrow convergence line strengthened on collision with the western slopes of the Black Forest. WRF failed to reproduce an elevated gust front, but convection (albeit weaker than observations) initiated above the mountain crests. Less precipitation occurred both above the mountains and further downstream. Errors in the model were largely attributed poor boundary-layer representation, which caused WRF to differ from the observations in two ways. The simulated boundary-layer was found to have a large dry bias, and a weaker convergence line formed in the lee of the Black Forest due to the inability to generate a south-easterly thermally-driven flow. Both factors created a troposphere that was insufficiently buoyant to reproduce the magnitude of the observed regenerated convection. Despite model errors, the key flow features were successfully reproduced and convection initiated above the crests of the northern Black Forest.

An idealised simulation that replaced the orography of the inner domain with a flat plain of equal height to that of the Rhine Valley found that in the absence of the Black Forest, the enhanced decay of convection in the lee of the Vosges was maintained, enabling considerable evolution of the MCS outflow into a density current when compared to R1. The undercutting of warm moist valley air was subsequently greater and a large area of valley air was lifted into the free troposphere. Convection, however, failed to regenerate as it had in R1. Ahead of the outflow, the gust front was still present but as a far weaker feature. When the leading edge of the outflow eventually reached the orography of the Swabian Jura convection regeneration was instantaneous. We therefore suggest that the following two mechanisms were necessary for convection to regenerate above the Black Forest.

1. The lifting of warm, moist air above mountain height by an undercutting outflow;

2. The strengthening and organisation of a gust front due to its collision with significant orography.

Studies such as C11 and Kalthoff et al. (2011) revealed that flows within the Black Forest valleys are important for the details of the convection initiation. However for regeneration simply to occur, a second idealised simulation that replaced the inner domain orography with an idealised three-dimensional ridge showed that the complexity of orography was unimportant and that it was solely the presence of significant orography that was required. Comparison of R3 with R1 showed more intense and a more southerly extent of convection was associated with a longer and more intense convergence line. This was attributed to the steeper and more uniform gradient of the upstream western slope of the ideal orography. In the southern part of the inner domain of R3, the ridge dropped away, forming a gap between the ridge and the orography of the southern Black Forest. The MCS outflow was channelled through this gap, allowing the outflow air to encounter the orography of the south-westerly part of the Swabian Jura. It was this convergence that allowed the mesoscale convergence line and convection to extend further south in R3 compared to R1.

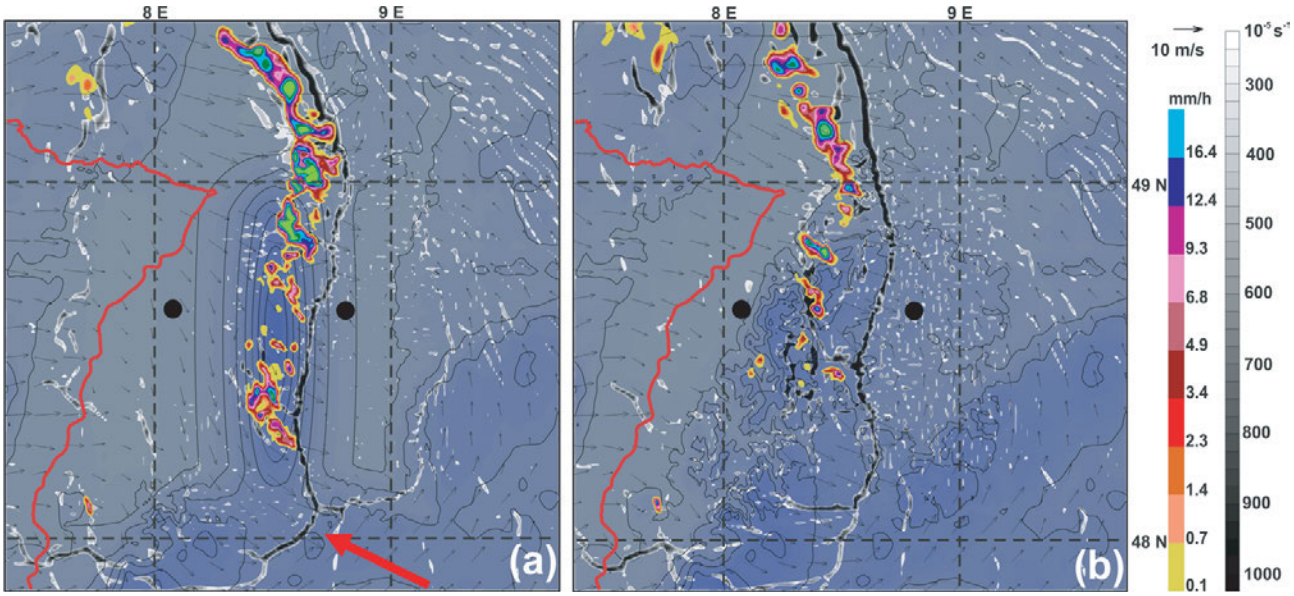

Figure 14: Same as Fig. 13 but for R3 (a) and R1 (b) at 1120 UTC. The red in (a) arrow indicates channelling of surface flows between the southern part of the idealised ridge and the southern Black Forest.

6 Conclusions

The WRF numerical model has revealed that convection regenerated above the crests of the Black Forest mountains on 20 July 2007 because of the additional uplift provided by the orography, when warm and moist Rhine Valley air was lifted by the undercutting cold outflow of a mesoscale convective system. Two simulations with idealised topography revealed that the shape of the orography was unimportant for convection regeneration. Instead, inadequacies of all three simulations were found to stem from poor boundary-layer representations. We therefore recommend that future studies on convection initiation and regeneration focus on better representation of the boundary layer and not the orography.

Acknowledgements

The authors would like to thank the UK Natural Environment Research Council (NERC) and the German Research Foundation for funding this work and the Austrian Science Fund (FWF): Project: CONSTANCE (P19658-N10) for funding the deployment of the Vienna AWS mesonet.

References

Banta, R., 1990: The role of mountain flows in making clouds. In: Atmospheric Processes over Complex Terrain. Meteor Mono **45**, Amer. Meteor Soc., 229–283.

Barthlott, C., U. Corsmeier, C. Meissner, F. Braun, C. Kottmeier, 2006: The influence of mesoscale Circulation systems on triggering convective cells over complex terrain. – Atmos. Res. **81** 150–175.

Browning, K., A. Blyth, P. Clark, C. Corsmeier, C. Morcrette et al., 2007: The Convective Storm Initiation Project. – Bull. Amer. Meteor Soc. **88**, 1939–1955.

Burton R.R., A. Gadian, A. Blyth, S.D. Mobbs, 2013: Modelling isolated deep convection: A case study from COPS. – Meteorol. Z. **22**, 433–443.

Corsmeier, U., N. Kalthoff, C. Barthlott, A.D. Behrendt, P. Di Girolamo, M. Dorninger, J. Handwerker, C. Kottmeier, H. Mahlke, S. Mobbs, V. Smith, G. Vaughan, J. Wickert, V. Wulfmeyer, 2011: Driving processes for deep convection over complex terrain: A multi-scale analysis of observations from COPS-IOP9c. – Quart. J. Roy. Meteor Soc. **137** 137–155.

Crook, A., D. Tucker, 2005: Flow Over Heated Terrain. Part I: Linear theory and idealized numerical simulations. – Mon. Wea. Rev. **133** 2252–2564.

Di Girolamo, P., D. Summa, R. Ferretti, 2009: Rotational Raman Lidar measurements for the characterization of stratosphere-troposphere exchange mechanisms. – J. Atmos. Ocean. Tech **26**, 1742–1762.

Hong, SY., Y. Noh, J. Dudhia, 2006: A new vertical diffusion package with an explicit treatment of entrainment processes. – Mon. Wea. Rev. **134** 2318–2341.

Kalthoff, N., B. Adler, C. Barthlott, U. Corsmeier, S. Mobbs S Crewell, K. Traeumner, C. Kottmeier, A. Wieser, V. Smith, P. Di Girolamo, 2009: The impact of convergence zones on the initiation of deep convection: A case study from COPS. – Atmos. Res. **93** 680–694.

Kalthoff, N., M. Kohler, C. Barthlott, B. Adler, S. Mobbs, U. Corsmeier, K. Traeumner, T. Foken, R. Eigenmann, L. Krauss, S. Khodayar, P. Di Girolamo, 2011: The dependence of convective-related parameters on surface and boundary layer conditions over complex terrain. – Quart. J. Roy. Meteor. Soc. **137** 70–80.

Kunz, M., M. Puskeiler, 2010: High-resolution assessment of the hail hazard over complex terrain from radar and insurance data. – Meteorol. Z. **19** 427–439.

Lean, H., N. Roberts, P. Clark, C. Morcrette, 2009: The Surprising role of Orography in the Initiation of an Isolated Thunderstorm in Southern England. – Mon. Wea. Rev. **137** 3026–3046.

Meissner, C., N. Kalthoff, M. Kunz, G. Adrian, 2007: Initiation of shallow convection in the Black Forest mountains. – Atmos. Res. **86** 42–60.

Morcrette, C., H. Lean, K. Browning, J. Nicol, N. Roberts, P. Clark, A. Russell, A. Blyth, 2007: Combination of mesoscale and synoptic mechanisms for triggering an isolated thunderstorm: Observational case study of CSIP IOP 1. – Mon. Wea. Rev. **135** 3728–3749.

Skamarock, W., J. Klemp, J. Dudhia, D. Gill, D. Barker, M. Duda, X.Y. Huang, J. Powers, 2008: A Description of the Advanced Research WRF Version 3. – Technical Report NCAR/TN-475+STR, National Center for Atmospheric Research, Box 3000, Boulder, CO 80307.

Steinacker, R., M. Ratheiser, B. Bica, B. Chimani, M. Dorninger, W. Gepp, C. Lotteraner, S. Schneider, S. Tschannett, 2006: A Mesoscale Data Analysis and Downscaling Method over Complex Terrain. – Mon. Wea. Rev. **134** 2758–2771.

Weckwerth, T., D. Parsons, S. Koch, J. Moore, M. LeMone, B. Demoz, C. Flamant, B. Geerts, J. Wang, W. Feltz, 2004: An overview of the International H_2O project (IHOP_2002) and some preliminary highlights. – Bull. Amer. Meteor. Soc. **85** 253–277.

Weisman, M.L., C. Davis, W. Wang, K.W. Manning, J.B. Klemp, 2008: Experiences with 0–36-h explicit convective forecasts with the WRF-ARW model. – Wea. Forecast **23**, 407–437.

Wulfmeyer, V., A. Behrendt, et al., 2008: The Convective and Orographically-induced Precipitation Study A Research and Development Project of the World Weather Research Program for Improving Quantitative Precipitation Forecasting in Low-Mountain Regions. – Bull. Amer. Meteor. Soc. **89**, 1477–1486.